Lifetime Heterogeneity of DNA-Bound dppz Complexes Originates from Distinct Intercalation Geometries Determined by Complex-Complex Interactions

ARTICLE *in* INORGANIC CHEMISTRY · JANUARY 2013

Impact Factor: 4.76 · DOI: 10.1021/ic302626d · Source: PubMed

6 AUTHORS, INCLUDING:

Johanna Andersson
Chalmers University of Technology
13 PUBLICATIONS **211** CITATIONS
SEE PROFILE

Louise H Fornander
Chalmers University of Technology
9 PUBLICATIONS **74** CITATIONS
SEE PROFILE

Maria Abrahamsson
Chalmers University of Technology
29 PUBLICATIONS **717** CITATIONS
SEE PROFILE

Eimer M Tuite
Newcastle University
43 PUBLICATIONS **1,928** CITATIONS
SEE PROFILE

Inorganic Chemistry

Article

pubs.acs.org/IC

Lifetime Heterogeneity of DNA-Bound dppz Complexes Originates from Distinct Intercalation Geometries Determined by Complex–Complex Interactions

Johanna Andersson, Louise H. Fornander, Maria Abrahamsson, Eimer Tuite,[†] Pär Nordell,[‡] and Per Lincoln*

Department of Chemical and Biological Engineering, Chalmers University of Technology, SE-41296 Gothenburg, Sweden

ABSTRACT: Despite the extensive interest in structurally explaining the photophysics of DNA-bound $[Ru(phen)_2dppz]^{2+}$ and $[Ru(bpy)_2dppz]^{2+}$, the origin of the two distinct emission lifetimes of the pure enantiomers when intercalated into DNA has remained elusive. In this report, we have combined a photophysical characterization with a detailed isothermal titration calorimetry study to investigate the binding of the pure Δ and Λ enantiomers of both complexes with $[poly(dAdT)]_2$. We find that a binding model with two different binding geometries, proposed to be symmetric and canted intercalation from the minor groove, as recently reported in high-resolution X-ray structures, is required to appropriately explain the data. By assigning the long emission lifetime to the canted binding geometry, we can simultaneously fit both calorimetric data and the binding-density-dependent changes in the relative abundance of the two emission lifetimes using the same binding model. We find that all complex–complex interactions are slightly unfavorable for Δ-$[Ru(bpy)_2dppz]^{2+}$, whereas interactions involving a complex canted away from a neighbor are favorable for the other three complexes. We also conclude that Δ-$[Ru(bpy)_2dppz]^{2+}$ preferably binds isolated, Δ-$[Ru(phen)_2dppz]^{2+}$ preferably binds as duplets of canted complexes, and that all complexes are reluctant to form longer consecutive sequences than triplets. We propose that this is due to an interplay of repulsive complex–complex and attractive complex-DNA interactions modulated by allosteric DNA conformation changes that are largely affected by the nature of the ancillary ligands.

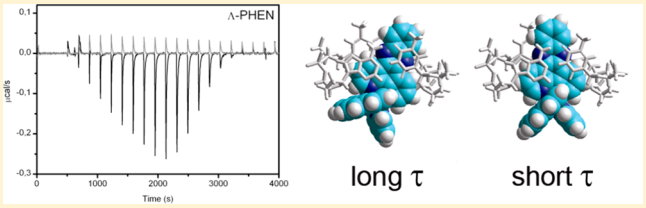

INTRODUCTION

In the pioneering work by Barton and Sauvage, it was first discovered that $[Ru(bpy)_2dppz]^{2+}$ (BPY; bpy = 2,2′-bipyridine, dppz = dipyrido[3,2-*a*:2′,3′-*c*]phenazine, Figure 1) exhibits bright luminescence when bound to DNA, although it is completely quenched in aqueous solution.[1,2] Shortly after this first observation, such "light-switch" properties in the presence of DNA was also observed for $[Ru(phen)_2dppz]^{2+}$ (PHEN, phen =1,10-phenanthroline),[3,4] where the bipyridines have been replaced by phenanthrolines. The DNA binding and spectroscopic properties of numerous structural analogues of the two prototype complexes have since been evaluated in pursuit of developing dppz-based complexes into useful reporter molecules for DNA.[4−9] The distinctive light-switch effect is generally considered to follow from protection of the phenazine nitrogens from hydrogen bonding water when the dppz moiety is intercalated between the base pairs; however, despite extensive photophysical studies on DNA-bound dppz complexes, with focus on the prototype compounds BPY and PHEN, there are fundamental questions still to be answered regarding their emission properties in the presence of DNA.

Early photophysical studies in our laboratory showed that the pure Δ and Λ enantiomers of both BPY and PHEN exhibit biexponential excited-state emission decays when bound to mixed-sequence DNA, as well as the synthetic polynucleotides $[poly(dAdT)]_2$ and $[poly(dGdC)]_2$, indicative of binding in microenvironments with different solvent accessiblility.[3,10] However, since biexponential decays are also observed upon binding to the more homogeneous polynucleotides poly-

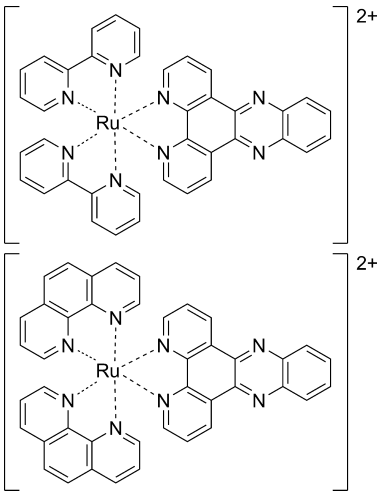

Figure 1. Structures of BPY (top) and PHEN (bottom).

Received: November 30, 2012
Published: December 26, 2012

   dx.doi.org/10.1021/ic302626d | *Inorg. Chem.* 2013, 52, 1151−1159

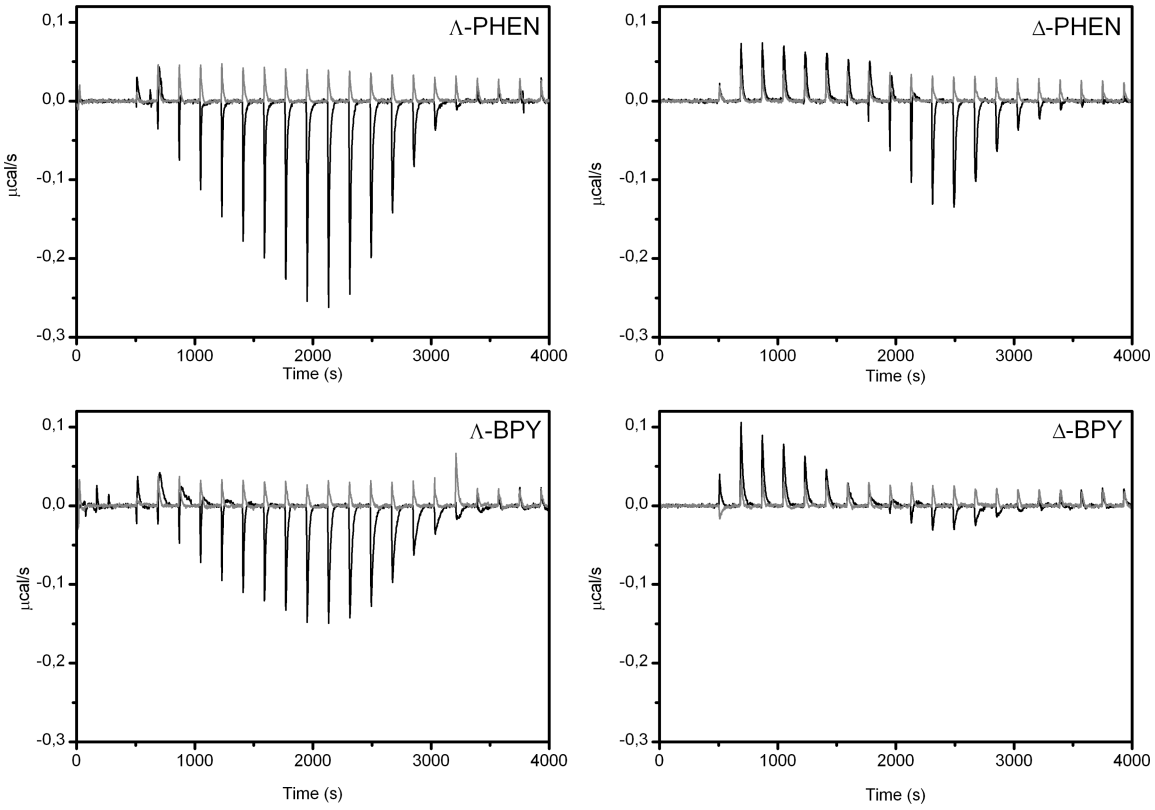

Figure 2. ITC raw data for binding of the Λ and Δ enantiomers of PHEN and BPY to $[poly(dAdT)]_2$ in 150 mM NaCl aqueous solution at 20 °C. Complex (~670−690 μM) was injected in 2 μL aliquots to the 206 μL cell containing the DNA (~200 μM base pairs). The heat of complex dilution is shown in gray.

(dA)·poly(dT) and poly(dG)·poly(dC), it was concluded that the two emission lifetimes could not simply be an effect of the base sequence around the intercalation pocket.[11] Furthermore, it was found that the relative contributions from the two emitting species change with binding density.[3,11,12]

The two emission lifetimes have been proposed to originate from two distinct orientations of the dppz moiety in the intercalation pocket, with intercalation occurring from the major groove.[4,13−17] The short emission lifetime was assigned to a canted, side-on, binding geometry, based on the possibility that one of the phenazine nitrogens of the intercalated dppz ligand is more readily accessible to water in such a binding geometry. Recently, Cardin and co-workers published a crystal structure of Λ-PHEN bound to a 10-mer oligonucleotide, which reveals two distinct intercalation geometries: one centered in the intercalation pocket and one with a more canted orientation, which indeed support the assignment of the two emission lifetimes to separate binding geometries.[18] However, in the crystal structure, intercalation occurs from the minor groove, which has also been observed for similar dppz complexes by NMR;[19,20] therefore, it is not obvious that the short emission lifetime should be assigned to the canted geometry. Moreover, the compact crystal structure may not be a true reflection of the structures found in aqueous solution. Thus, despite these new findings, it is still not clear if and how the two binding modes arise in solution, how they are related to the two emission lifetimes, and why the relative abundance of the two emission lifetimes changes with binding density.

In the present work, we have studied binding of the pure enantiomers of both PHEN and BPY to $[poly(dAdT)]_2$, using isothermal titration calorimetry (ITC). By combining ITC and excited-state lifetime data with theoretical binding isotherm models based on McGhee−von Hippel conditional probabilities, we assign the two emission lifetimes to their respective intercalation geometry and explain the binding-density-dependent variations in their relative abundance with a binding model that is consistent with crystallography and NMR data.

RESULTS

Isothermal Titration Calorimetry. The enthalpic part of the binding free energy can be directly assessed from the heat produced or absorbed upon addition of the ligand to a solution of DNA in a high-precision isothermal calorimetry experiment. ITC measurements were carried out at 15, 20, 25, and 30 °C in 150 mM NaCl aqueous solution, for which profiles were obtained by 19 sequential injections of ligand (the Δ and Λ enantiomers of PHEN and BPY) from a syringe stock solution into the sample cell loaded with $[poly(dAdT)]_2$. The concentration ranges used for ligand and DNA were set to span mixing ratios [ligand]/[base pair] from 0.05 to 0.7. Raw data from representative ITC experiments at 20 °C is shown in Figure 2.

The ITC profile typically expected when a ligand is added to a macromolecule with a single type of nonoverlapping binding sites has, from a low degree of saturation to a high degree of saturation, a sigmoidal shape with an initial plateau, followed by a transition region that eventually reaches a second plateau.[21] The first injections reflect the enthalpy of the interaction as virtually all of the injectant (injected ligand) binds the macromolecule in the first plateau region. In the transition region, the affinity and stoichiometry of ligand binding govern the shape of the binding isotherm. When the system eventually

dx.doi.org/10.1021/ic302626d | Inorg. Chem. 2013, 52, 1151−1159

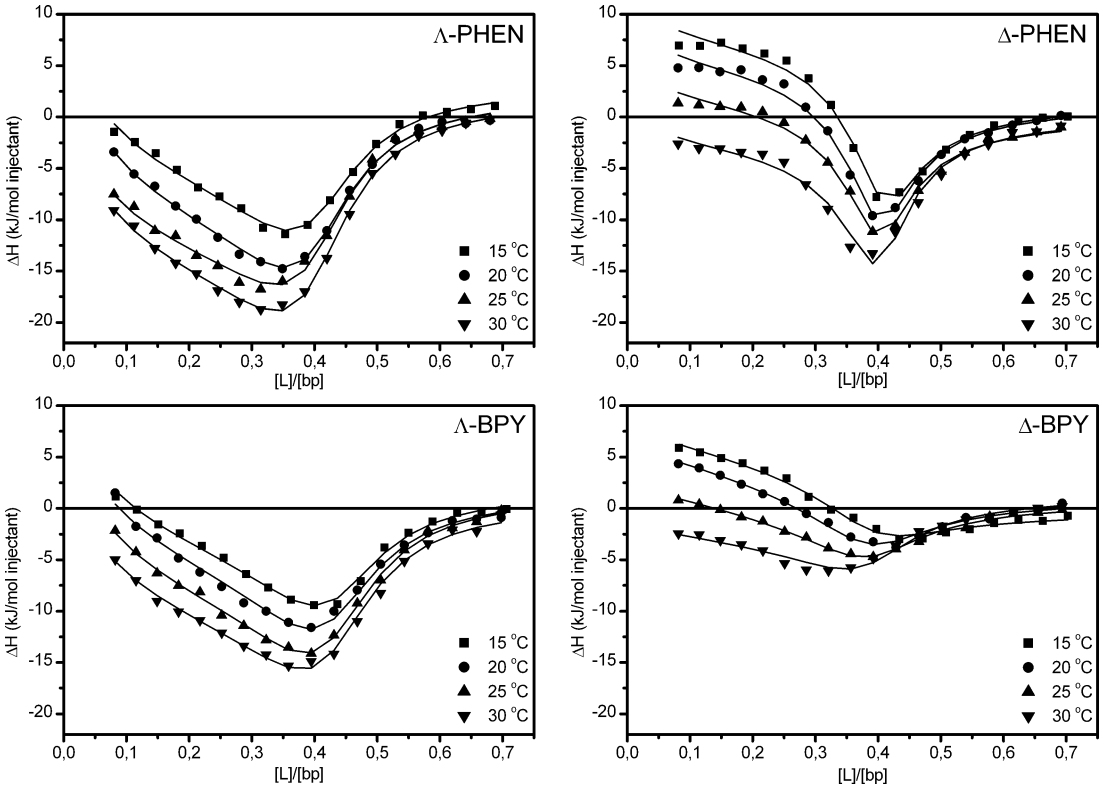

Figure 3. ITC profiles with fitted traces for the binding of Λ and Δ enantiomers of PHEN and BPY to $[poly(dAdT)]_2$ in 150 mM NaCl aqueous solution. Symbols indicate the normalized integrated heat absorbed or evolved upon sequential 2 μL injections of complex (~670–690 μM) into the 206 μL cell containing the DNA (~200 μM base pairs). The data have been corrected for heat of dilution of the complex.

reaches saturation, a further increase of ligand concentration does not result in any further binding, giving the second plateau in the ITC diagram.

Interestingly, we observe that the obtained ITC profiles deviate strongly from this standard shape in the low-saturation regime (Figure 3). Following the initial injection, for which binding generally is associated with low enthalpies (within the range of ±4 kJ/mol injectant), binding gradually becomes more exothermic, reaching a negative maximum at [L]/[bp] = 0.3–0.4, where affinity and saturation starts to limit the amount of injectant bound. From the shapes of the ITC profiles, it appears that at least two different types of binding interactions are present for all four complexes, where the second one, which mainly occurs when the DNA lattice starts to become saturated, is associated with a more negative enthalpy than the first one. The profiles for the Λ enantiomers share common features in both shape and magnitude, whereas the differences to and between the Δ enantiomers are obvious. In contrast to the Λ enantiomers, Δ-PHEN displays an initial plateau of constant injection heat, reaching a mixing ratio of ~0.25 before binding becomes exothermic. The signals for Δ-BPY are much weaker compared to the other three complexes.

Photophysics. The excited-state emission decays of Λ- and Δ-PHEN and BPY bound to $[poly(dAdT)]_2$ were determined at mixing ratios of [L]/[bp] = 0.1, 0.33 and 0.67, corresponding to the low-, intermediate-, and high-saturation regime of the ITC profiles. Each decay could satisfactorily be fitted to a biexponential expression, giving the two lifetimes τ_1 and τ_2 and the corresponding normalized pre-exponential factors α_1 and α_2 presented in Table 1.

The two Λ enantiomers display similar photophysical profiles. For both, the contribution from the dominating short-lived component (~50 ns) decreases gradually (from $\alpha_1 \approx 0.65$ to $\alpha_1 \approx 0.35$) over the three [L]/[bp] ratios. The Δ enantiomers exhibit larger differences. In agreement with earlier reports,[3,11,22] we obtain much longer lifetimes (170 and 850 ns) and a much higher proportion of the long-lived component ($\alpha_2 \approx 0.6$ already at [L]/[bp] = 0.1) for Δ-PHEN. For Δ-BPY, on the other hand, α_2 is much lower, compared to the other complexes, at all binding ratios, with a maximum value of ~0.3 at [L]/[bp] = 0.67.

Table 1. Photophysical Data at Different Binding Ratios

	ratio	τ_1	α_1	τ_2	α_2
Δ-PHEN	0.1	161	0.43	838	0.57
	0.33	192	0.30	881	0.70
	0.67	167	0.26	842	0.74
Δ-BPY	0.1	107	0.85	338	0.15
	0.33	121	0.78	451	0.22
	0.67	119	0.72	447	0.28
Λ-PHEN	0.1	47	0.65	326	0.35
	0.33	48	0.49	329	0.51
	0.67	48	0.33	295	0.67
Λ-PBY	0.1	49	0.64	325	0.36
	0.33	55	0.49	330	0.51
	0.67	55	0.41	301	0.59

Development of a Binding Model To Fit Calorimetric and Photophysical Data Simultaneously. In contrast to proteins, where binding of a ligand generally occurs only at very specific and isolated binding sites, DNA can be seen as a long

dx.doi.org/10.1021/ic302626d | Inorg. Chem. 2013, 52, 1151–1159

polymer of closely spaced binding sites for an intercalating ligand. If the ligand covers, or otherwise makes inaccessible, more than one base pair when bound to the DNA, the binding sites effectively overlap each other, which necessitates the use of a McGhee and von Hippel type of method to calculate the binding isotherms.[23] Furthermore, direct or indirect (allosteric) interactions between neighboring ligands can either facilitate binding of an adjacent ligand (cooperativity) or make adjacent binding less favorable (anticooperativity). In order to simultaneously model the ITC and photophysical data, a binding model with several binding parameters was required. We start by discussing the limitations of simple models to explain the evolution of the final model.

In the simplest case (Figure 4, Model 1a), a single type of DNA binding geometry (denoted C) is assumed, and the

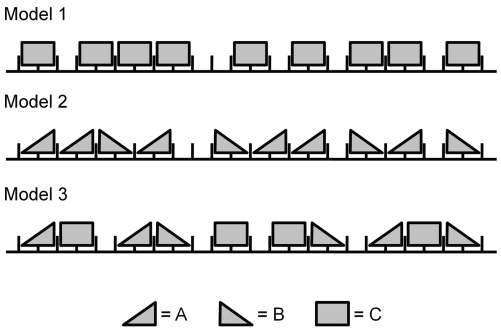

Figure 4. Schematic illustration of the different binding models.

binding of one ligand next to an already bound ligand is set to be neither cooperative nor anticooperative (i.e., noncooperative; $y_{CC} = 1$, see the Methods section). To account for the two types of binding enthalpy indicated by the ITC data, the model assumes an *intrinsic binding enthalpy*, ΔH, for each bound ligand ($\Delta H \approx \Delta H^{\circ}$, neglecting non-ideality of the solutes), and an *interaction enthalpy*, Δh, for each pair of adjacently bound ligands. However, this simple model resulted in poor fits to the ITC curves. To improve the fits, the cooperativity parameter y_{CC} was allowed to be non-unity, and this model (1b) gave satisfactory simulation of ITC curves (not shown) using 3 adjustable parameters (the intrinsic binding constant (K), the binding site exclusion parameter (n) and the cooperativity parameter (y_{CC})).

Since Model 1b is based on a single binding mode, lifetime heterogeneity must be ascribed to ligand–ligand interactions. However, no assignment of the two excited-state lifetimes to ligands with or without neighbors could explain their relative fractions (normalized pre-exponential factors) as a function of the ratio. When the fit of Model 1b to the ITC data indicates that the binding of contiguous ligands is cooperative ($y_{CC} > 1$), as for the PHEN and BPY Λ enantiomers, essentially all ligands would be contiguously bound at saturation. Hence, only one emission lifetime would be expected at high binding ratios, contrary to what is observed. Conversely, when the Model 1b fit indicates anticooperative ligand interactions ($y_{CC} < 1$), as for Δ-PHEN, most ligands would bind without neighbors at low binding ratios. Hence, one dominating emission lifetime would be expected, with the second emission lifetime not appearing until the DNA is close to saturation, in further disagreement with the observed behavior.

By considering the simplest situations, we see that a binding model that can take into account bound ligands having both cooperative and anticooperative interactions is needed. One such model is obtained by assuming unsymmetric binding of the ligand giving rise to a pair of polar elementary units A and B, such that the nearest-neighbor interaction in one direction along the DNA helix is different from the interaction in the opposite direction (Model 2). This model requires five adjustable parameters to calculate the binding isotherm (K, n, $y_{AA} = y_{BB}$, y_{AB}, and y_{BA}). However, since this model also assigns lifetime heterogeneity to ligand–ligand interactions, it fails to correctly predict the lifetime distribution close to saturation of the DNA (data not shown).

Having excluded the previous models, we conclude that the binding of BPY and PHEN to DNA must give rise to more than one binding geometry. Our proposed scheme, Model 3, assumes that DNA ligands bound with only one nearest-neighbor have one distinct, unsymmetrical binding geometry (denoted A or B, depending on whether it appears in the beginning or at the end of a contiguous sequence, respectively), and that ligands bound in a symmetric environment (either isolated, or with nearest-neighbors on both sides) have a second binding geometry denoted C. Furthermore, we assume that the lifetime depends only on the binding geometry, but that binding enthalpies are influenced by interactions with neighboring ligands. This binding model can be treated in the McGhee–von Hippel framework as two formally distinct ligands (though coupled through the mass balance equations; see eq 6 in the Methods section) competing for the same binding sites on a one-dimensional lattice. Since not all cooperativity parameters are unity, the matrix-based generalized McGhee–von Hippel method is required to calculate the binding isotherms and model the data.[24]

Following the notation defined in the Methods section, the binding geometries are denoted as elementary units A, B, and C, where elementary unit C is nonpolar, and A and B are polar elementary units (cooperativity parameter $y_{AB} \neq y_{BA}$). Because of the 2-fold symmetry of the DNA-lattice, A and B are otherwise identical and they will thus have the same excited-state lifetime. Elementary units A and B are allowed only at the start and the end, respectively, of a contiguous sequence of bound ligands. Thus, most cooperativity parameters involving A and B are zero: $y_{AF} = y_{FB} = y_{AA} = y_{BB} = y_{BA} = y_{CA} = y_{BC} = 0$ (F denotes a free binding site). The binding site coverage parameter n is allowed to take non-integer values and to be different between C and A/B. Since A and B cannot exist isolated in the model, K_A (= K_B), y_{AC} (= y_{CB}), and y_{AB} will not be independent parameters, and therefore K_A was set equal to $^1/_2K_C$ (where the factor $^1/_2$ is due to the assumed 2-fold symmetry of the C binding geometry).[24] At a particular temperature, the intrinsic binding enthalpy ΔH is assumed to have the same value for all binding geometries (A, B, and C). Also, the interaction enthalpy Δh for neighboring ligands is assumed to have the same value whenever the interior elementary unit C is involved (AC, CB, and CC) but is set to zero for the AB interaction. Therefore, Model 3 has six adjustable parameters for the binding isotherm itself (K, n_A, n_B, y_{AB}, y_{AC}, and y_{CC}) and two additional for the fit to the ITC curves (ΔH and Δh).

As shown in Figures 3 and 5, this model provides an excellent fit to both ITC data and emission lifetime α-values, as long as A/B is identified with the long excited-state lifetime and C with the short. Table 2 presents the values of the binding isotherm parameters that give the best fit, and Figure 6 show the values of ΔH and Δh obtained from the least-squares fit to the ITC

dx.doi.org/10.1021/ic302626d | Inorg. Chem. 2013, 52, 1151–1159

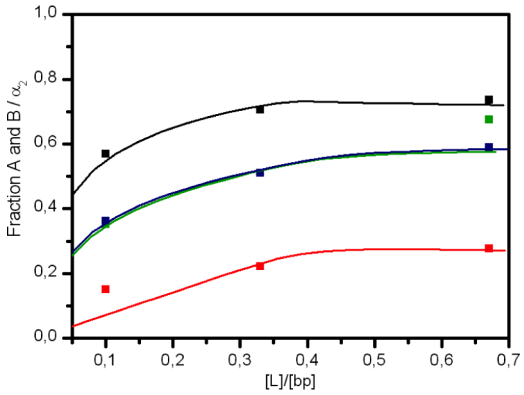

Figure 5. Comparison of the calculated fractions of A and B (solid lines) with the pre-exponential factors for the long emission lifetimes (squares) for Δ-PHEN (black), Δ-BPY (red), Λ-PHEN (green), and Λ-BPY (blue).

Table 2. Binding Parameters That Give the Best Fit to Experimental Data

complex	K ($\times 10^6$ M^{-1})	y_{AB}	y_{AC}	y_{CC}	n_A	n_C
Δ-PHEN	1.1	56	6	0.01	2	1.8
Δ-BPY	1.3	0.3	0.6	0.2	2	1.8
Λ-PHEN	0.2	8	9	0.05	2	1.8
Λ-BPY	0.2	10	9	0.05	1.85	1.65

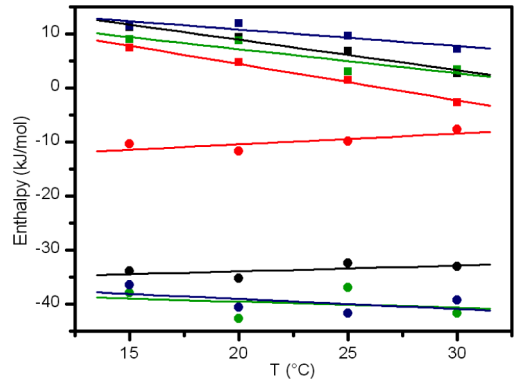

Figure 6. Intrinsic binding enthalpies ΔH (squares) and interaction enthalpies Δh (circles) for binding of Δ-PHEN (black), Δ-BPY (red), Λ-PHEN (green), and Λ-BPY (blue) to $[poly(dAdT)]_2$ in 150 mM NaCl at different temperatures. The slopes of the fitted lines correspond to the ΔC_p for the reactions.

curves as a function of temperature. Table 3 gives the thermodynamic parameters for the intrinsic binding of the four different complexes to $[poly(dAdT)]_2$ at 20 °C, where ΔC_P is obtained from the least-squares linear fits shown in Figure 6.

Table 3. Thermodynamic Parameters for the Intrinsic Binding at 20 °C

complex	$\Delta G°$ (kJ mol^{-1})	$\Delta H°$ (kJ mol^{-1})	$\Delta S°$ (J K^{-1} mol^{-1})	ΔC_p (J K^{-1} mol^{-1})
Δ-PHEN	−33.9	7.4	140	−570
Δ-BPY	−34.3	4.5	130	−670
Λ-PHEN	−29.8	7.2	130	−450
Λ-BPY	−29.8	10.9	140	−310

DISCUSSION

By simultaneously analyzing calorimetric and photophysical data, we find that a binding model involving two differently bound species, one of them being polar, i.e., asymmetric, with respect to adjacent sites, is required to simultaneously fit both datasets. Although slightly better fits might be achieved with even more-detailed models, we consider that this minimal satisfactory model, common for all complexes and constructed with as few parameters as possible, most readily facilitates comparison of the effects of ruthenium ligand structure and chirality on binding. In the following, we discuss the physical implications of the proposed binding model.

Binding Geometry and Excited-State Lifetime. The simplest model that can satisfactorily fit both ITC and emission lifetime data requires two distinct binding modes, one polar (A/B) and one symmetric (C). In light of the recent crystal structure presented by Cardin and co-workers,[18] it is reasonable to identify the polar binding mode as a canted intercalation geometry and the symmetrical species as complexes intercalated in the center of the intercalation pocket. Furthermore, it is necessary to assign the long lifetime to the polar end-units A and B, and the short one to the symmetric unit C, which supports the hypothesis that the different lifetimes are a direct consequence of distinct binding geometries, rather than a result of steric shielding from quenching water when ligands bind in close proximity to each other. Our assignment of lifetimes is opposite to the previous hypothesis,[4] though, in which the side-on geometry was assigned to the short lifetime since one phenazine nitrogen exposed in the major groove appeared to be readily accessible to hydrogen bonding by water molecules. However, that intercalation model placed the $Ru(phen)_2$-moiety in the major groove, resulting in a more shallow intercalation and thus a larger angle between the complex 2-fold axis and the intercalation pocket dyad axis than in the canted geometry suggested by Cardin's crystal structure, where intercalation occurs from the minor groove.[18]

We cannot exclude the possibility that intercalation occurs from the major groove in solution, as has been suggested from competition experiments and one ^1H NMR study.[13−17] However, since it is possible that the binding of the complex may be altered in competition experiments,[25] and, to the best of our knowledge, no structural data for major groove intercalated dppz complexes exist yet, we consider that minor groove intercalation is more likely also in solution. We base this on our previous work on PHEN in solution,[11,26] and the fact that minor groove intercalation have been observed for several dppz complexes in both NMR studies[19,20] and recent crystal structures.[18,27,28] By assuming intercalation to occur from the minor groove, we can also rationalize the assignment of the long emission lifetime to the canted geometry.

Examination of molecular models of minor groove intercalated PHEN (Figure 7) suggests that one phenazine nitrogen is virtually hidden and the other one exposed in the major groove for the canted A/B geometries, whereas both nitrogens are symmetrically exposed for the C geometry. Since studies on the excited-state quenching dynamics as function of temperature of free PHEN in polyol solvents indicate that hydrogen bonding to both phenazine nitrogens is required to completely quench the luminescence, this supports the assignment of the long lifetime to the unsymmetrical binding geometry A/B.[29] Importantly, regardless of the groove preferences of the complexes, it is still necessary to assign the

dx.doi.org/10.1021/ic302626d | Inorg. Chem. 2013, 52, 1151−1159

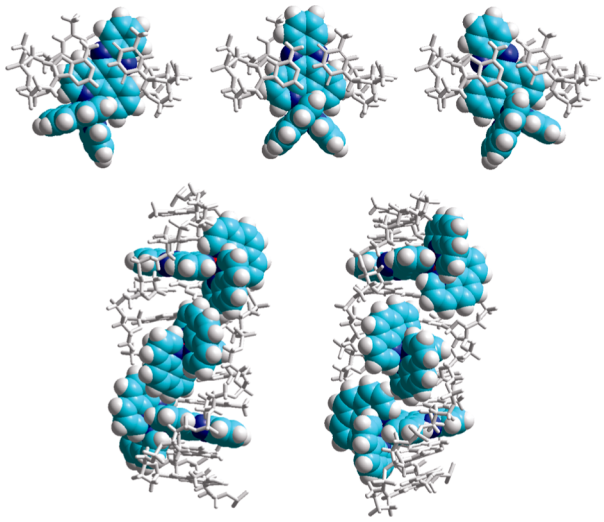

Figure 7. Schematic illustration of the proposed interaction geometries. Top: View along the helix axis (from above) of the A (left), the symmetric C (middle), and B (right) binding geometries for Λ-PHEN. Bottom: View along the central base pair dyad axis of the sequence A–C–B for Δ-PHEN (left) and Λ-PHEN (right). The models were constructed by manual docking and subsequent energy minimization in vacuo, using the AMBER 2 force field in the HyperChem 7.52 software package (HyperCube, Inc.).

long emission lifetime to the polar unit A/B to simultaneously fit both datasets, and our binding model would still hold, even if intercalation occurs from the major groove in solution.

Cooperative Binding. Since the cooperativity parameters determine the equilibrium between the two postulated binding geometries, it is evident that ligand–ligand interactions are responsible for the variations in the relative abundance of the long and short emission lifetimes with binding ratio. In terms of cooperativity parameters, Δ-BPY is distinctive in exhibiting modest anticooperativity for all ligand–ligand interactions, indicating that this complex has a slight preference for binding isolated with the symmetrical binding mode C. The similar magnitude of the three cooperativity parameters indicates that for this particular complex, in fact, a simple binding model in which the long lifetime is ascribed to accidental neighbors would suffice. By contrast, the other three complexes show both cooperative (the AC/CB and AB interactions) and anticooperative (the CC interaction) behavior, suggesting that they readily form ACB triplets that very reluctantly expand to larger consecutive sequences. This should theoretically give α_2 values of ∼0.67 at saturation, which is more or less what is observed at [L]/[bp] = 0.67 (see Figure 5). Δ-PHEN stands out, with its much larger AB cooperativity parameter, which indicates that, at low binding densities, this ligand prefers forming AB pairs, i.e., doublets in which the two complexes are canted away from each other, minimizing the direct phenanthroline–phenanthroline interactions.

Apparently, the ancillary ruthenium ligands have great influence on the cooperativity and, hence, the photophysical behavior of the investigated complexes when bound to DNA. An important consequence of this result is that PHEN and BPY cannot be used interchangeably in DNA binding studies, as has been commonly assumed in the literature, but should be treated as distinct DNA binding drugs. We note that biphasic calorimetry isotherms over similar binding ratios have previously been reported for several racemic $[Cr(diimine)_2dppz]^{3+}$ complexes with calf thymus DNA.[30] Differences between the ITC profiles of $[Cr(phen)_2dppz]^{3+}$ and $[Cr(bpy)_2dppz]^{3+}$ are observed also in this study, although they are not as striking as those between the pure Δ enantiomers of PHEN and BPY observed here.

However, what is even more interesting is the ITC profile for $[Cr(TMP)_2dppz]^{3+}$ (TMP = 3,4,7,8-tetramethyl-1,10-phenanthroline), which is significantly different from those of the phenanthroline and bipyridine complexes. The binding of $[Cr(TMP)_2dppz]^{3+}$ can be modeled with only one type binding site, further emphasizing that small differences in ancillary ligand structure have large effect on the DNA interaction. Also $[Ru(tpm)(dppz)py]^{2+}$ and $[Ru(tpm)(dppz)py\text{-}R]^{2+}$ (tpm = tripyridazole methane, py = pyridine, and py-R = 4-substituted pyridine) have recently been shown to exhibit significantly different ITC profiles.[31] It is plausible to assume that this effect extends to other dppz compounds with different arrangements and sizes of the ancillary ligands, e.g., $[Ru(tpy)(dppz)(py\text{-}R)]^{2+}$ (tpy = 2,2′:6′,2″-terpyridine).[32] Thus, dppz complexes with different ancillary ligands are likely to exhibit different cooperativity patterns, which might influence their potential use as drugs or reporter molecules for DNA.

Ligand–Ligand Interactions. While the extra hydrophobic area represented by the fused benzene ring of phenanthroline does not seem to influence the intrinsic binding constants of the four complexes or the cooperativity parameters for the Λ enantiomers, the effect is dramatic concerning the cooperativity parameters for the Δ enantiomers. The CC interaction becomes much more anticooperative, and the AC and AB interactions become much more cooperative when going from Δ-BPY to Δ-PHEN. The direct physical interaction between two complexes is greatest in the CC arrangement. In view of the molecular model of the ACB interactions shown in Figure 7, it seems plausible that the fused benzene ring of phenanthroline will come into even closer contact with at least the fused pyridine ring of the neighboring Δ complexes in the CC arrangement, resulting in steric and electrostatic repulsion.

This attribution of anticooperativity to the physical close contact between neighboring complexes indicates that the strong increase in cooperativity in the AB interaction for Δ-PHEN has its origin in a favorable interactions between the fused benzene ring and the DNA backbone in the canted binding geometry. The similar values of y_{AC} (0.6 for BPY and 6 for PHEN) and the square root of y_{AB} (0.55 for BPY and 7.5 for PHEN), suggests that this may indeed be the case, since y_{AC} involves one interaction and y_{AB} involves two such interactions. However, the question is then why, given the favorable interaction with the DNA backbone, does the canted A or B geometry not occur for individual isolated Δ-PHEN molecules? We propose that allosteric conformational changes, caused by binding of another complex, are necessary to allow the canted binding geometry, but that the cooperative effect of those changes are more or less canceled out by anticooperative ligand–ligand interactions. Thus, the major contribution to the cooperativity parameters y_{AC} and y_{AB} is the favorable interactions between the canted complexes and the DNA backbone, but these interactions are not possible without preceding conformational changes of the DNA.

Although the intrinsic binding constant have been shown to be strongly dependent on ionic strength,[33] the pre-exponential factors obtained at low salt (5 mM phosphate buffer) for similar binding ratios appear to be roughly the same as those observed

dx.doi.org/10.1021/ic302626d | Inorg. Chem. 2013, 52, 1151–1159

here,[12] indicating that the cooperativity parameters are less sensitive to salt concentration.

Binding Parameters and Thermodynamics. All complexes exhibit small positive ΔH and negative ΔC_p values. This means that ΔH will decrease to zero within or close to the temperature range studied here ($\Delta H = 0$ between 27 °C and 45 °C), where the intrinsic binding constant K will reach a maximum. As a consequence, the variation of K in this temperature range is predicted to be small (±4%), justifying the use of a constant value for K in the fit of the model to binding isotherms at the different temperatures. As shown in Figure 6, the interaction enthalpy Δh, which can be assigned almost entirely to the AC interaction, is large and negative (−37 ±5) kJ K^{-1} mol^{-1} (except for Δ-BPY) and shows significantly weaker temperature dependence than ΔH. Although the large negative value of Δh indicates that the corresponding equilibrium constants (the cooperativity parameter y_{AC} and y_{CC}) should change by approximately ±25% within the temperature range employed, we did not find it warranted to include the modest temperature dependence of these parameters into the binding isotherm model in view of the simplifying assumptions regarding the origin of Δh in the model.

The positive ΔH shows that the intrinsic binding of all complexes is entropically driven at room temperature, and the observation of negative heat capacity changes upon binding, ΔC_p, suggest that burying hydrophobic surfaces from solvent accessibility gives an important contribution to binding affinity.[34,35] The intrinsic binding enthalpies for the PHEN enantiomers are of the same order of magnitude as those determined by Haq et al. in a previous ITC study for binding to mixed-sequence calf thymus DNA at 50 mM NaCl and 20 °C (+1.0 kJ/mol and +12 kJ/mol for Δ and Λ, respectively), while the binding constants are slightly larger than those obtained from luminescence titrations using a simple binding model in the same study (~2.5 × 10^5 for Δ and ~1.7 × 10^5 M^{-1} for Λ-PHEN at 150 mM NaCl).[33] However, since the complexes have a preference for AT-base pairs,[15] the binding constants are indeed expected to be larger with $[poly(dAdT)]_2$ and our results seems reasonable in comparison with the findings by Haq et al.

Moreover, the best-fit values of the binding site exclusion parameters, $n_{A/B}$ and n_C, were for all complexes found to be close to the nearest-neighbor exclusion value commonly found for classical intercalators ($n = 2$), even though they were allowed to vary independently. Since the polar subunits were defined to always have a free binding site F on one side, either to the left for A or to the right for B, their effective binding site exclusion will be larger but dependent on the type of next-neighboring subunit. If y_{CC} is taken to be zero, the maximum binding density $\theta_{L,max}$ in the limit of free ligand concentration approaching infinity (the theoretical saturation value), can readily be calculated from the arrangement with the maximum number of ligands per lattice binding site. As discussed above, this arrangement is a sequence of ACB triplets interspaced by single free binding sites (...ACBFACBFACBF...) for all complexes except Δ-BPY, which gives $\theta_{L,max} = n_{avg}^{-1} = [(2 + 1.8 + 2 + 1)/3]^{-1} = 0.44$ using the n values determined for Model 3 (see Table 2). This results in an average binding site exclusion parameter $n_{avg} = 2.27$, which is comparable to the reported value for Δ-PHEN binding to $[poly(dAdT)]_2$ determined by fitting Model 1b to a binding isotherm obtained by luminescence titration ($n = 2.3$).[36]

CONCLUSIONS

By a combined analysis of calorimetric and photophysical data for binding of the pure Δ and Λ enantiomers of $[Ru(phen)_2dppz]^{2+}$ and $[Ru(bpy)_2dppz]^{2+}$ to $[poly(dAdT)]_2$, using the generalized McGhee−von Hippel method, we have been able to assign the two emission lifetimes to two distinct intercalation geometries. The short lifetime is attributed to complexes centered in the intercalation pocket, whereas the long lifetime arises from a canted binding geometry found only at the ends of contiguous sequences of bound ligands. We suggest that an interplay of repulsive interligand and favorable DNA backbone interactions modulated by allosteric changes in DNA conformation accounts for the simultaneous cooperative and anticooperative features of the binding, resulting in predominant formation of only short contiguous sequences of bound ligands. Interestingly, this study shows that, although the dppz moiety is an important feature for introducing intercalation properties to metal polypyridyl complexes, the ancillary ligands greatly influence the binding characteristics of such compounds. Therefore, the PHEN and BPY complexes cannot be used interchangeably in DNA binding studies, as is generally assumed in the literature.

METHODS

Materials and Sample Preparation. $[Ru(phen)_2dppz]Cl_2$ and $[Ru(bpy)_2dppz]Cl_2$ were synthesized according to the procedure previously reported by Hiort et al.,[3,37] and stock solutions (~5 mM) were prepared by dissolving the chloride salts in MQ water. All experiments were performed in a buffer solution containing 150 mM NaCl and 1 mM sodium cacodylate (pH 7.0). A stock solution of $[poly(dAdT)]_2$ (~5 mM) was prepared by dissolving the sodium salt purchased from Sigma−Aldrich in buffer. For ITC measurements, the DNA solution was dialyzed against buffer using a dialysis membrane with a molecular weight cutoff of 6000−8000 Da (Spectra/Por, Spectrum Laboratories, Inc.) for at least 48 h at 8 °C. Ruthenium complex solutions were then prepared by dilution of the stock solutions in the dialysate. Concentrations were determined spectrophotometrically using ε_{262} = 6600 M^{-1} cm^{-1} per nucleotide for $[poly(dAdT)]_2$, ε_{439} = 20 000 M^{-1} cm^{-1} for PHEN,[3] and ε_{444} = 16 100 M^{-1} cm^{-1} for BPY.[38]

Isothermal Titration Calorimetry. Calorimetric data was obtained using an ITC 200 isothermal titration calorimeter (MicroCal, Inc., USA) controlled by Origin 7.0 software by titrating 2.0 μL aliquots of ruthenium complexes (670−690 μM) into 206 μL of DNA solution (~400 μM nucleotides). The heat change associated with the titration was determined by integrating the power required to maintain the reference and sample cells at the same temperature. The primary ITC data was corrected for the heat of ligand dilution by subtracting the average heat per injection of ruthenium complex titrated into the buffer. Heat arising from DNA dilution was negligible. Experiments were performed at 15, 20, 25, and 30 °C, and for the experiments performed at 30 °C, the samples were degassed under vacuum for 5 min prior to loading.

Emission Lifetime Measurements. The emission decays were measured with a Nd:YAG laser (Continuum Surelite II-10, pulse width <7 ns) pumping an optical parametric oscillator set to an excitation wavelength of 457 nm. The emitted light was collected through a monochromator set to 616 nm and detected by a Hamamatsu R928 photomultiplier tube perpendicular to the excitation light. Decay traces were collected and averaged by a 200 MHz digital oscilloscope (Tetronix TDS2200 2Gs/s), and stored by a LabView program. The time-resolved data was analyzed with a biexponential decay function:

$$I(t) = \alpha_1 \exp\left(-\frac{t}{\tau_1}\right) + \alpha_2 \exp\left(-\frac{t}{\tau_1}\right)$$

dx.doi.org/10.1021/ic302626d | Inorg. Chem. 2013, 52, 1151−1159

The Generalized McGhee–von Hippel Binding Model for One Ligand with Multiple Binding Modes to an Infinite One-Dimensional Lattice. Since it is a long polymer chain of alternating, stacked base pairs with intercalation pockets between each base pair, $[poly(dAdT)]_2$ can, neglecting the difference between the dA-dT and dT-dA steps, be treated as an infinite linear lattice, the subunits of which are the identical binding sites. Because of the alternating sequence, the intercalation pockets will possess 2-fold symmetry, making the subunits and the lattice itself nonpolar. Using the notation by Chen,[39] the lattice with bound ligands can be described as a heteropolymer of N types of elementary units of varying length, where the length n_i is defined as the number of subunits that the elementary unit i contains. Elementary unit 1 is the free binding site (naked lattice subunit); thus, $n_1 = 1$, and lengths of the other $N - 1$ elementary units will be dependent on the number of free binding sites that are covered, physically or otherwise made inaccessible, by the bound ligand. The binding density (θ_i) is defined as the ratio between the number of elementary units being of type i, relative to the total number of subunits (binding sites, B). Thus, the total binding density of a ligand L (θ_L), which is defined as the ratio of bound ligand to the total concentration of binding sites, is given by $\theta_L = [\text{bound L}]/[B]_{total} = \sum \theta_i$, where the summation is restricted to elementary units i that contain L. Correspondingly, the density of type 1 units (free binding sites) is given as $\theta_1 = 1 - \sum n_i\theta_i$. Taking an arbitrary direction along the lattice to define the sequence of elementary units, when elementary unit i is followed by j on the lattice, the net cooperativity parameter y_{ij} is related to the nearest-neighbor interaction free energy (ϖ_{ij}) as

$$y_{ij} = \exp\left(- \frac{[\varpi_{ij} - \varpi_{11}]}{kT} \right) \quad (1)$$

where ϖ_{11} is the nearest-neighbor interaction free energy between two naked lattice subunits and k is the Boltzmann constant. The conditional probability p_{ij} is the probability that, given a randomly chosen elementary unit of type i, the immediately following unit will be of type j. The conditional probabilities are the elements of the $N \times N$ matrix $\mathbf{P}$, which is a stochastic matrix since each row sum is unity: $\sum_{j=1} p_{ij} = 1$. Thus, the column vector $\mathbf{e} = [1\ 1 \ldots 1]$ is a right-hand eigenvector to $\mathbf{P}$ with eigenvalue 1, and it can be shown that the corresponding left-hand eigenvector is the row vector of binding densities $\boldsymbol{\theta}^T = [\theta_1 \ldots \theta_N]$, where ^{T} indicates transposition, thus[24]

$$\mathbf{Pe} = \mathbf{e} \quad \text{and} \quad \boldsymbol{\theta}^T\mathbf{P} = \boldsymbol{\theta}^T \quad (2)$$

Let $\mathbf{Y}$ be the matrix of cooperativity parameters y_{ij}; the relationship between $\mathbf{P}$ and $\mathbf{Y}$ then is given by the factorization

$$\mathbf{P} = \mathbf{SYR} \quad (3)$$

where $\mathbf{S}$ and $\mathbf{R}$ are two diagonal matrices with positive diagonal elements s_{ii} and r_{ii}, respectively. The binding potential x_i, that determines the equilibrium between elementary unit i, a consecutive sequence of n_i free binding sites and free ligand L, is readily expressed in terms of s_{ii}, r_{ii}, and p_{11} (the conditional probability for a free site to be followed by another free site):

$$x_i = K_i[L] = s_{ii}r_{ii}p_{11}^{-ni}\ x_1 \equiv 1 \quad (4)$$

where K_i is the intrinsic binding constant and [L] denotes the concentration of free ligand L.

Because of the 2-fold symmetry of the binding site, a ligand that itself possesses C_2 symmetry will give rise to a single, unpolar elementary unit a only if the symmetry axes of the ligand and the binding site coincide. Otherwise, the binding will give rise to a pair of polar elementary units a and b, for which $K_a = K_b$, $n_a = n_b$, and $y_{aa} = y_{bb}$ but $y_{ab} \neq y_{ba}$, and, upon interaction with a nonpolar elementary unit c, $y_{ac} = y_{cb} \neq y_{ca} = y_{bc}$. Given $\mathbf{Y}$ and θ, under the condition that eq 2 will hold, eq 3 can be solved iteratively as described earlier.[24] Given the total concentration of binding sites $[B]_{total}$ and the binding constant K_i, for each of the equilibria, the total concentration of ligand can be calculated as

$$[L]_{total,i} = [L]_i + [\text{bound L}] = x_iK_i^{-1} + \theta_L[B]_{total} \quad (5)$$

where $[L]_{total,i}$ and $[L]_i$ are the total and free ligand concentrations, respectively, calculated from the equilibrium involving elementary unit i.

Thus, starting with an initial guess of the binding density vector $\boldsymbol{\theta}$, for a given total concentration of added ligand $[L]_{added}$, the elements of the error vector $\mathbf{q}$ can be calculated:

$$q_i = [L]_{total,i} - [L]_{added} \quad (6)$$

Since the matrix of derivatives $\partial x_i/\partial\theta_j$ can readily be constructed, an efficient Newton–Raphson procedure can be devised for the minimization of $\mathbf{q}$ and, hence, calculation of the binding isotherm with $\boldsymbol{\theta}$ as a function of $[B]_{total}$ and $[L]_{added}$, satisfying the mass balance equations described by eq 6 and the equilibria determined by the given values of y_{ij}, K_i, and n_i.[24]

For simulation of ITC curves, the change in concentration of total bound ligand $\theta_L[B]_{total}$ upon each injection of ligand was calculated, as well as the change in concentration of bound ligands with nearest-neighbor interactions, thought to give rise to the interaction enthalpy change Δh. Since the lattice is nonpolar, $\theta_ip_{ij} = \theta_jp_{ji}$, and the concentration of nearest-neighbor interacting ligands were calculated as the sum of $\theta_ip_{ij}[B]_{total}$ for the i–j interactions of interest. The heat of injection data were then projected in a least-squares sense on the space spanned by the calculated total ligand and the interaction change vectors, allowing as well for a constant baseline value, to give the calculated reaction enthalpies.

AUTHOR INFORMATION

Corresponding Author

*Tel.: +46 31 772 30 55. Fax: +46 31 772 38 58. E-mail: lincoln@chalmers.se.

Present Addresses

†School of Chemistry, Bedson Building, Newcastle University, Newcastle upon Tyne NE1 7RU, U.K.

‡DMPK Innovative Medicines, AstraZeneca R&D Mölndal, Sweden.

Notes

The authors declare no competing financial interest.

ACKNOWLEDGMENTS

The authors gratefully acknowledge COST action D35 and Swedish Research Council (VR) for support.

REFERENCES

(1) Friedman, A. E.; Chambron, J. C.; Sauvage, J. P.; Turro, N. J.; Barton, J. K. *J. Am. Chem. Soc.* **1990**, *112*, 4960–4962.

(2) Amouyal, E.; Homsi, A.; Chambron, J. C.; Sauvage, J. P. *J. Chem. Soc., Dalton Trans.* **1990**, 1841–1845.

(3) Hiort, C.; Lincoln, P.; Norden, B. *J. Am. Chem. Soc.* **1993**, *115*, 3448–3454.

(4) Hartshorn, R. M.; Barton, J. K. *J. Am. Chem. Soc.* **1992**, *114*, 5919–5925.

(5) Andersson, J.; Li, M. N.; Lincoln, P. *Chem.—Eur. J.* **2010**, *16*, 11037–11046.

(6) Li, M. N.; Lincoln, P. *J. Inorg. Biochem.* **2009**, *103*, 963–970.

(7) McKinley, A. W.; Lincoln, P.; Tuite, E. M. *Coord. Chem. Rev.* **2011**, *255*, 2676–2692.

(8) Svensson, F. R.; Matson, M.; Li, M.; Lincoln, P. *Biophys. Chem.* **2010**, *149*, 102–106.

(9) Wilhelmsson, L. M.; Westerlund, F.; Lincoln, P.; Norden, B. *J. Am. Chem. Soc.* **2002**, *124*, 12092–12093.

(10) Lincoln, P. Ph.D. Thesis, Chalmers University of Technology, 1998.

(11) Tuite, E.; Lincoln, P.; Norden, B. *J. Am. Chem. Soc.* **1997**, *119*, 239–240.

(12) McKinley, A. W.; Andersson, J.; Lincoln, P.; Tuite, E. M. *Chem.—Eur. J.* **2012**, *18*, 15142−15150.
(13) Dupureur, C. M.; Barton, J. K. *J. Am. Chem. Soc.* **1994**, *116*, 10286−10287.
(14) Dupureur, C. M.; Barton, J. K. *Inorg. Chem.* **1997**, *36*, 33−43.
(15) Holmlin, R. E.; Stemp, E. D. A.; Barton, J. K. *Inorg. Chem.* **1998**, *37*, 29−34.
(16) Jenkins, Y.; Friedman, A. E.; Turro, N. J.; Barton, J. K. *Biochemistry* **1992**, *31*, 10809−10816.
(17) Turro, C.; Bossmann, S. H.; Jenkins, Y.; Barton, J. K.; Turro, N. J. *J. Am. Chem. Soc.* **1995**, *117*, 9026−9032.
(18) Niyazi, H.; Hall, J. P.; O'Sullivan, K.; Winter, G.; Sorensen, T.; Kelly, J. M.; Cardin, C. J. *Nat. Chem.* **2012**, *4*, 621−628.
(19) Greguric, A.; Greguric, I. D.; Hambley, T. W.; Aldrich-Wright, J. R.; Collins, J. G. *J. Chem. Soc., Dalton Trans.* **2002**, 849−855.
(20) Waywell, P.; Gonzalez, V.; Gill, M. R.; Adams, H.; Meijer, A. J. H. M.; Williamson, M. P.; Thomas, J. A. *Chem.—Eur. J.* **2010**, *16*, 2407−2417.
(21) Jelesarov, I.; Bosshard, H. R. *J. Mol. Recognit.* **1999**, *12*, 3−18.
(22) Olofsson, J.; Wilhelmsson, L. M.; Lincoln, P. *J. Am. Chem. Soc.* **2004**, *126*, 15458−15465.
(23) McGhee, J. D.; von Hippel, P. H. *J. Mol. Biol.* **1974**, *86*, 469−489.
(24) Lincoln, P. *Chem. Phys. Lett.* **1998**, *288*, 647−656.
(25) Yun, B. H.; Kim, J. O.; Lee, B. W.; Lincoln, P.; Norden, B.; Kim, J. M.; Kim, S. K. *J. Phys. Chem. B* **2003**, *107*, 9858−9864.
(26) Lincoln, P.; Broo, A.; Norden, B. *J. Am. Chem. Soc.* **1996**, *118*, 2644−2653.
(27) Hall, J. P.; O'Sullivan, K.; Naseer, A.; Smith, J. A.; Kelly, J. M.; Cardin, C. J. *Proc. Natl. Acad. Sci.* **2011**, *108*, 17610−17614.
(28) Song, H.; Kaiser, J. T.; Barton, J. K. *Nat. Chem.* **2012**, *4*, 615−620.
(29) Olofsson, J.; Onfelt, B.; Lincoln, P. *J. Phys. Chem. A* **2004**, *108*, 4391−4398.
(30) Vandiver, M. S.; Bridges, E. P.; Koon, R. L.; Kinnaird, A. N.; Glaeser, J. W.; Campbell, J. F.; Priedemann, C. J.; Rosenblatt, W. T.; Herbert, B. J.; Wheeler, S. K.; Wheeler, J. F.; Kane-Maguire, N. A. P. *Inorg. Chem.* **2010**, *49*, 839−848.
(31) Walker, M. G.; Gonzalez, V.; Chekmeneva, E.; Thomas, J. A. *Angew. Chem., Int. Ed.* **2012**, *51*, 12107−12110.
(32) Zhou, Q.-X.; Yang, F.; Lei, W.-H.; Chen, J.-R.; Li, C.; Hou, Y.-J.; Ai, X.-C.; Zhang, J.-P.; Wang, X.-S.; Zhang, B.-W. *J. Phys. Chem. B* **2009**, *113*, 11521−11526.
(33) Haq, I.; Lincoln, P.; Suh, D. C.; Norden, B.; Chowdhry, B. Z.; Chaires, J. B. *J. Am. Chem. Soc.* **1995**, *117*, 4788−4796.
(34) Spolar, R. S.; Record, M. T. *Science* **1994**, *263*, 777−784.
(35) Ren, J. S.; Jenkins, T. C.; Chaires, J. B. *Biochemistry* **2000**, *39*, 8439−8447.
(36) Lincoln, P.; Tuite, E.; Norden, B. *J. Am. Chem. Soc.* **1997**, *119*, 1454−1455.
(37) Lincoln, P.; Norden, B. *J. Phys. Chem. B* **1998**, *102*, 9583−9594.
(38) Chambron, J. C.; Sauvage, J. P. *Chem. Phys. Lett.* **1991**, *182*, 603−607.
(39) Chen, Y. D. *Biopolymers* **1990**, *30*, 1113−1121.